Atmospheric Environment 48 (2012) 22–32

Contents lists available at SciVerse ScienceDirect

Atmospheric Environment

journal homepage: www.elsevier.com/locate/atmosenv

Aerosol properties of the Eyjafjallajökull ash derived from sun photometer and satellite observations over the Iberian Peninsula

C. Toledano [a,*], Y. Bennouna [a], V. Cachorro [a], J.P. Ortiz de Galisteo [a], A. Stohl [b], K. Stebel [b], N.I. Kristiansen [b], F.J. Olmo [c], H. Lyamani [c], M.A. Obregón [d], V. Estellés [e], F. Wagner [f], J.M. Baldasano [g], Y. González-Castanedo [a,h], L. Clarisse [i], A.M. de Frutos [a]

[a] Grupo de Optica Atmosferica, Universidad de Valladolid, Valladolid, Spain
[b] Norwegian Institute for Air Research, Kjeller, Norway
[c] Universidad de Granada, Granada, Spain
[d] Universidad de Extremadura, Badajoz, Spain
[e] Universidad de Valencia, Valencia, Spain
[f] University of Evora, Evora, Portugal
[g] Barcelona Supercomputing Center, Barcelona, Spain
[h] Departamento de Geología, Universidad de Huelva, Huelva, Spain
[i] Service de Chimie Quantique et Photophysique, Université Libre de Bruxelles, Brussels, Belgium

ARTICLE INFO

Article history:
Received 20 February 2011
Received in revised form
27 September 2011
Accepted 28 September 2011

Keywords:
Eyjafjallajökull
Sun photometer
AERONET
Optical properties
Remote sensing
FLEXPART

ABSTRACT

The Eyjafjallajökull ash that crossed over Spain and Portugal on 6–12 May 2010 has been monitored by a set of operational sun photometer sites within AERONET-RIMA and satellite sensors. The sun photometer observations (aerosol optical depth, coarse mode concentrations) and ash products from IASI and SEVIRI satellite sensors, together with FLEXPART simulations of particle transport, allow identifying the volcanic aerosols. The aerosol columnar properties derived from inversions were investigated, indicating specific properties, especially regarding the absorption. The single scattering albedo was high (0.95 at 440 nm) and nearly wavelength independent, although with slight decrease with wavelength. Other parameters, like the fine mode fraction of the volume size distributions (0.20–0.80) or the portion of spherical particles (15–90%), were very variable among the sites and indicated that the various ash clouds were inhomogeneous with respect to particle size and shape.

1. Introduction

The eruption of the Eyjafjallajökull volcano in southern Iceland (63.6°N, 19.6°W) began on 20 March 2010. On 14 April 2010 an explosive eruption started in the caldera beneath the Eyjafjallajökull ice cap. The northwesterly winds over Iceland transported the volcanic emissions towards northern Europe (starting with UK and Norway) (Petersen, 2010). The volcanic ash caused major disruption in air traffic in that week as it crossed over central Europe, where it was detected by different means (Ansmann et al., 2010; Schumann et al., 2011). After a quieter period during late April, the eruption intensified again on 3 May. In this case the ash was transported southwards over the Atlantic and part of the ash cloud turned to the east, affecting Portugal, Spain and France where some airports were closed on 6–8 and 10–12 May.

The Eyjafjallajökull eruption produced a tephra plume that reached a height of 9 km according to radar measurements from the Icelandic Meteorological Office (IMO). However the plume height was lower (5–7 km) most of the time and aerosols very seldom penetrated the stratosphere (Petersen, 2010).

Information on the Eyjafjallajökull eruption, such as description of the eruptive phases, plume heights, chemical and size distribution analysis, references, etc., can be found in the website of the Institute of Earth Sciences (http://www.earthice.hi.is/page/ies_Eyjafjallajokull_eruption). Preliminary investigations from the Environment Agency of Iceland indicated that 24% of the aerosol mass in ground samples was smaller than 10 μm (aerosols) and about 33% in the range 10–50 μm. During many periods the ash plume was sufficiently electrified to generate lightning (Bennett et al., 2010).

* Corresponding author.
E-mail address: toledano@goa.uva.es (C. Toledano).

1352-2310/$ – see front matter © 2011 Elsevier Ltd. All rights reserved.
doi:10.1016/j.atmosenv.2011.09.072

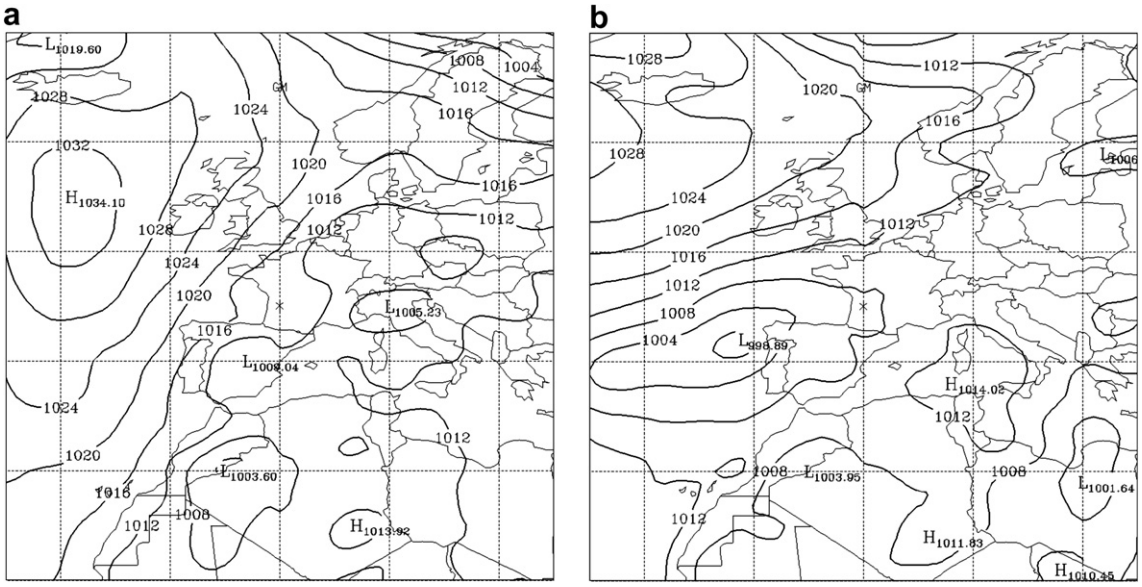

Fig. 1. Mean sea level pressure analysis on (a) 3 May 00UTC, showing the high pressure system south of Iceland that produced the meridional transport of volcanic aerosols; (b) 8 May 18UTC.

Large volcanic eruptions, like that of Mount Pinatubo in 1991, may influence climate (e.g. (Minnis et al., 1993)). Aerosols can be injected as high as 25 km, the decay of the stratospheric concentration lasting for years. The magnitude of the Eyjafjallajökull eruption was much smaller and the aerosol emission remained in the troposphere, where the particle lifetime is much shorter (removal processes are more intense) than in the stratosphere.

The disruption of air traffic highlighted the importance of real-time observations and forecast transport models (Stohl et al., 2011), to assess the ash extent and concentration. Models can also be validated offline and improved with the reported observations. Network observations of ash optical properties within the European Aerosol Lidar Network (EARLINET, (Ansmann et al., 2010; Pappalardo et al., 2010; Wiegner et al., in press))(lidar), the Aerosol Robotic Network (AERONET, (Ansmann et al., 2010))(sun photometer) or the Deutscher Wetterdienst (DWD) ceilometer network (Flentje et al., 2010) provided near real-time monitoring of the volcanic aerosols.

The aim of this paper is to investigate the optical and microphysical properties of the Eyjafjallajökull volcanic aerosols, based on the AERONET-RIMA (Iberian Network for Aerosol Measurements, federated to AERONET) sun photometer observations in the Iberian Peninsula during the period 6–12 May 2010. We used satellite and lidar data to identify the volcanic aerosols and the Lagrangian model FLEXPART to confirm the presence of these aerosols. Range resolved measurements (mainly lidars and ceilometers) are more suitable for the detection of aerosol layers in the free troposphere. However the AERONET global spatial coverage and real-time operational capabilities make worth investigating the sun photometer data during this volcanic aerosol event. These results can be compared with many sites and events, to provide valuable information about the aerosol properties and keys for correct interpretation when other measurements are not available.

It should be noted that the main difficulty with a sun photometer is that it provides information on the entire atmospheric column and cannot separate the volcanic aerosols from other particles within the boundary layer.

The paper is structured as follows: first a meteorological overview for the May event is provided (Section 2), followed by the description of the utilized measurements and methods (Section 3). Then the results are discussed (Section 4), starting with the satellite and model analysis, followed by the analysis of AOD from sun photometer and finally by the aerosol properties derived from the inversion of sun-sky radiance data. The conclusions are given in Section 5.

2. Meteorological situation

This section is focused on the meteorological conditions that produced the transport of aerosols from the Eyjafjallajökull volcano to the Iberian Peninsula on 6–12 May. An overview of the meteorology during the entire eruption period can be found in Petersen (2010).

The pressure charts on the days before 7 May show a strong high pressure system at the surface centered south of Iceland and east of the Irish coast (Fig. 1). At higher levels the isobars presented a typical omega shape, with high pressure over the east Atlantic Ocean and low pressure over the West Atlantic and Europe. This synoptic situation produced strong upper-level northerly winds

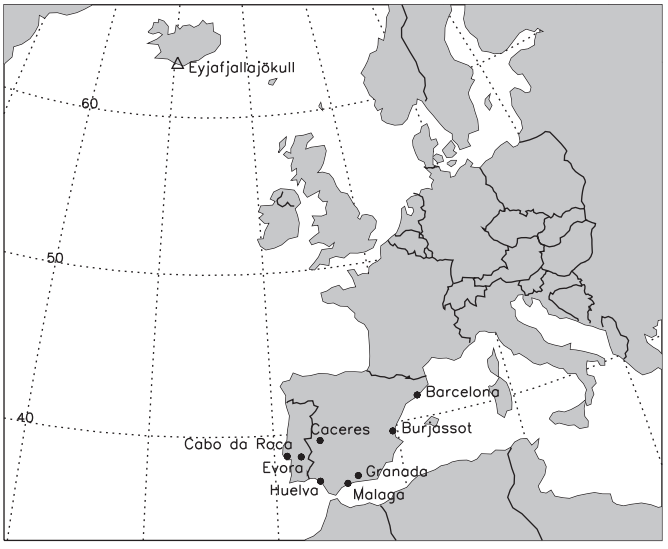

Fig. 2. Location of the AERONET-RIMA sun photometer sites in the Iberian Peninsula used in this study.

Table 1
AERONET-RIMA sites in the Iberian Peninsula used in the study of the volcanic ash on 6–12 May 2010. The typical aerosol background is indicated, as well as the database level in the AERONET archive and key references about the site characterization.

Site	Background aerosol	Data level	Remarks
Barcelona	Urban	2.0	Lidar; (Basart et al., 2009)
Burjassot	Urban	1.5	(Estellés et al., 2007)
Cabo da Roca	Marine	2.0	
Cáceres	Continental	2.0	(Obregón et al., 2009)
Evora	Continental	1.5	Lidar; (Elias et al., 2006)
Granada	Urban	1.5	Lidar; (Lyamani et al., 2004, 2005)
Huelva	Marine	1.5	(Bennouna et al., 2011; Toledano et al., 2007a, 2007b)
Málaga	Marine	1.5	(Foyo-Moreno et al., 2010)

over Iceland that transported the volcanic aerosols southwards over the North Atlantic. Then the wind turned westerly due to an upper-level low pressure system and flew over the Iberian Peninsula on 7 May.

On 7 May a low pressure system at the surface level and at higher levels, centered north of Spain, produced instability and abundant cloudiness and precipitations over the north half of Spain and Portugal. On 8 May, a frontal system associated with a low approaching from the west crossed over the Iberian Peninsula from southwest toward northeast (Fig. 1b). It was a cloudy and rainy day, especially in the western part.

The following days, the position of an upper-level trough weakened the meridional flow over Spain. This depression was located over the Atlantic Ocean close to the northwest coast of Spain, and it was accompanied by a low pressure system at the surface, producing southwesterly winds throughout the troposphere over Spain and Portugal. Several frontal systems crossed over the Iberian Peninsula. On 11 May, the low pressure system at the surface moved eastward and at high level the flow over the Iberian Peninsula turned northern. On 12 May the northerly flow at high level intensified. Finally, on 13 May a low pressure system at surface and at high levels moved over Iceland and the flow changed to zonal.

3. Observation sites and methodology

A number of AERONET sites, belonging to the RIMA subnetwork, operate in the Iberian Peninsula. The site locations are shown in Fig. 2. Due to cloudiness not all sites collected data during this episode. The sites that are used in our study are included in Table 1. A brief description of the sites is provided in http://www.caelis.uva.es/station.

The sun photometer sites are all equipped with Cimel sun–sky radiometers, the standard instruments of the AERONET network (Holben et al., 1998). These instruments have 9 channels covering the spectral range 340–1020 nm for the direct Sun measurements, and four channels (440, 670, 870 and 1020 nm) for the sky radiances (almucantar and principal plane). Direct Sun data are collected every 15 min and sky radiances are collected every hour. The Cimel instruments were calibrated according to the AERONET protocols,

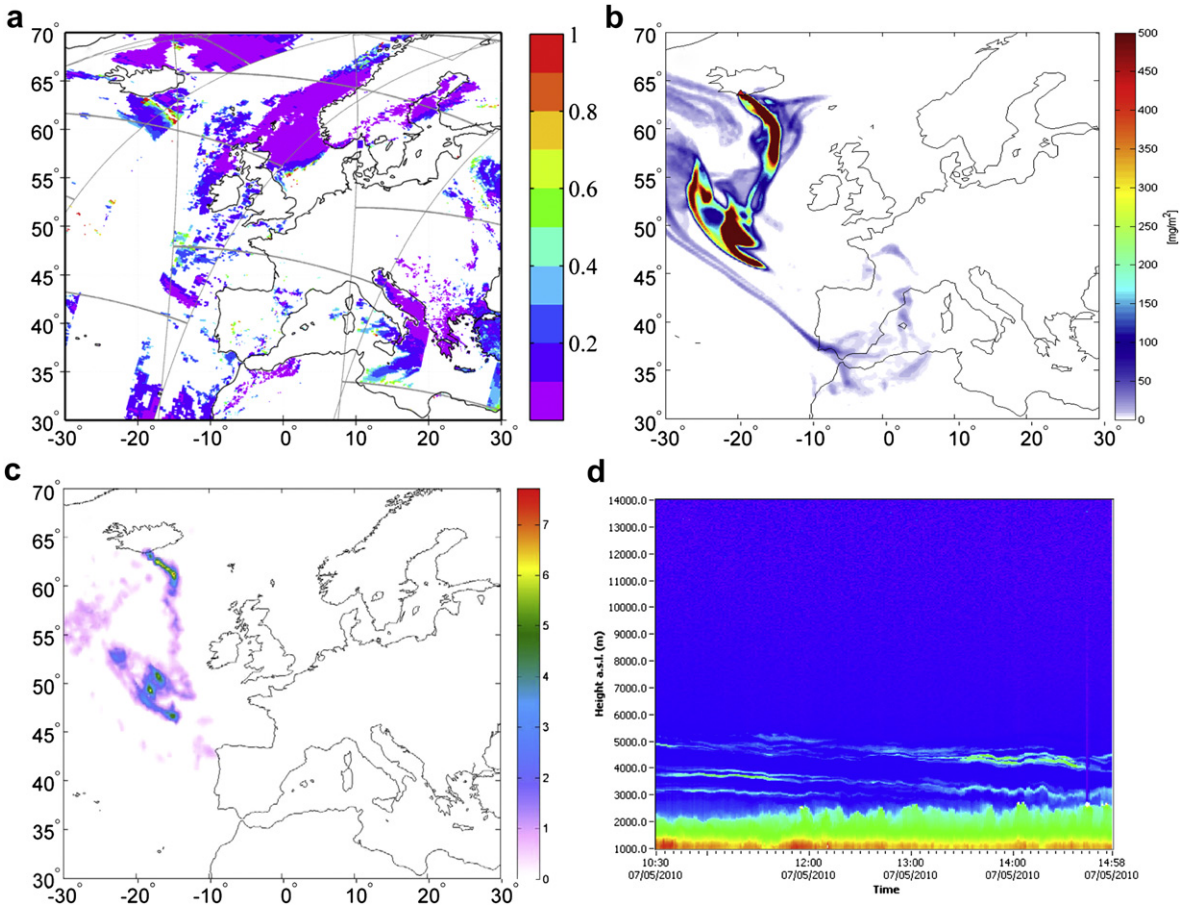

Fig. 3. (a) MODIS aerosol optical depth at 550 nm on 7 May 2010 (Terra); (b) FLEXPART simulation for column mass concentration at 1800UTC for particle size 0.75–2.5 μm; (c) Brightness temperature difference (K) from IASI satellite sensor at morning overpass (about 0930UTC); (d) Range corrected signal (arbitrary units) of the Granada lidar system (532 nm channel).

either at the RIMA calibration facility (Valladolid, Spain) or the PHOTONS facility (Lille, France). The absolute AOD uncertainty is 0.02 and the sky radiance error is 5%. The data were processed to derive spectral aerosol optical depth (AOD), following the Beer–Bouguer–Lambert law, Ångström exponent (AE), indicator of the AOD spectral dependence and related to particle size predominance, and a set of optical and microphysical parameters applying an inversion algorithm (Dubovik and King, 2000; Dubovik et al., 2000). The current model version (Dubovik et al., 2006) accounts for particle non-sphericity with a spheroid model and retrieves the portion of non-spherical particles of the aerosol size distribution (note, however, that volcanic ash particles, as well as desert dust particles, are very complex structures). See also Technical and Quality Assurance Documents in the AERONET website for further information.

The inversion products used in our analysis are the particle size distribution (PSD), single scattering albedo (SSA), complex refractive index and sphericity parameter (i.e. portion of spherical particles). The assessment studies by Dubovik et al. (2000) indicate the uncertainties associated to the various parameters. As for the size distributions, the errors range from 15 to 35% for 0.1 μm < r < 7 μm to 100% outside this interval. The single scattering albedo absolute error is 0.03. The optical properties (refractive indices and SSA) are quality-assured only if AOD (400 nm) is larger than 0.4. These conditions of having a moderately high AOD were not always fulfilled during the ash event over the Iberian Peninsula. Hence the AOD threshold was reduced to 0.25 at 440 nm wavelength, and the inversion results were carefully analyzed. The AERONET level 2.0 inversion data are still not available for all sites (Table 1). However, in order to increase the reliability of the level 1.5 inversion data, these were filtered with the level 2.0 quality criteria: solar zenith angle larger than 50°, retrieval error less than 5% (difference between observed and inverted sky radiances) and the minimum number of angles in the almucantar as indicated in AERONET's Version 2.0 quality assurance criteria (available at: http://aeronet.gsfc.nasa.gov/new_web/Documents/AERONETcriteria_final1.pdf).

To support the evidence of volcanic ash over the AERONET-RIMA sites, the standard Terra and Aqua Moderate Resolution Imaging Spectroradiometer (MODIS) level 2 aerosol products from collection 5.1, respectively the MOD04 and MYD04 provided by NASA GSFC (available at http://modis.gsfc.nasa.gov), were used (Levy et al., 2009). This product provides the aerosol optical depth and other aerosol properties (e.g. Ångström exponent, fine mode AOD fraction) over land and ocean at the spatial resolution of 10 × 10 km^2. In this paper, only the land–ocean AOD retrievals at 550 nm are presented. Spatial subsets of these MODIS data were extracted to select all pixels falling within a distance of 25 km from the AERONET location, and spatially averaged to obtain the data time series for MODIS. During the day, the Terra satellite overpasses the Iberian Peninsula roughly between 10 and 12 UTC in the morning, while Aqua overpass time is later in the afternoon between about 12 and 14 UTC. The AOD climatology derived from MODIS observations over the Iberian Peninsula, validated with ground-based AERONET data, was reported by (Bennouna et al., 2011).

Two more satellite sensors were used to investigate the arrival of puffs of ash. Based on infrared channels (Prata and Grant, 2001; Clarisse et al., 2010a), total column mass loadings were estimated

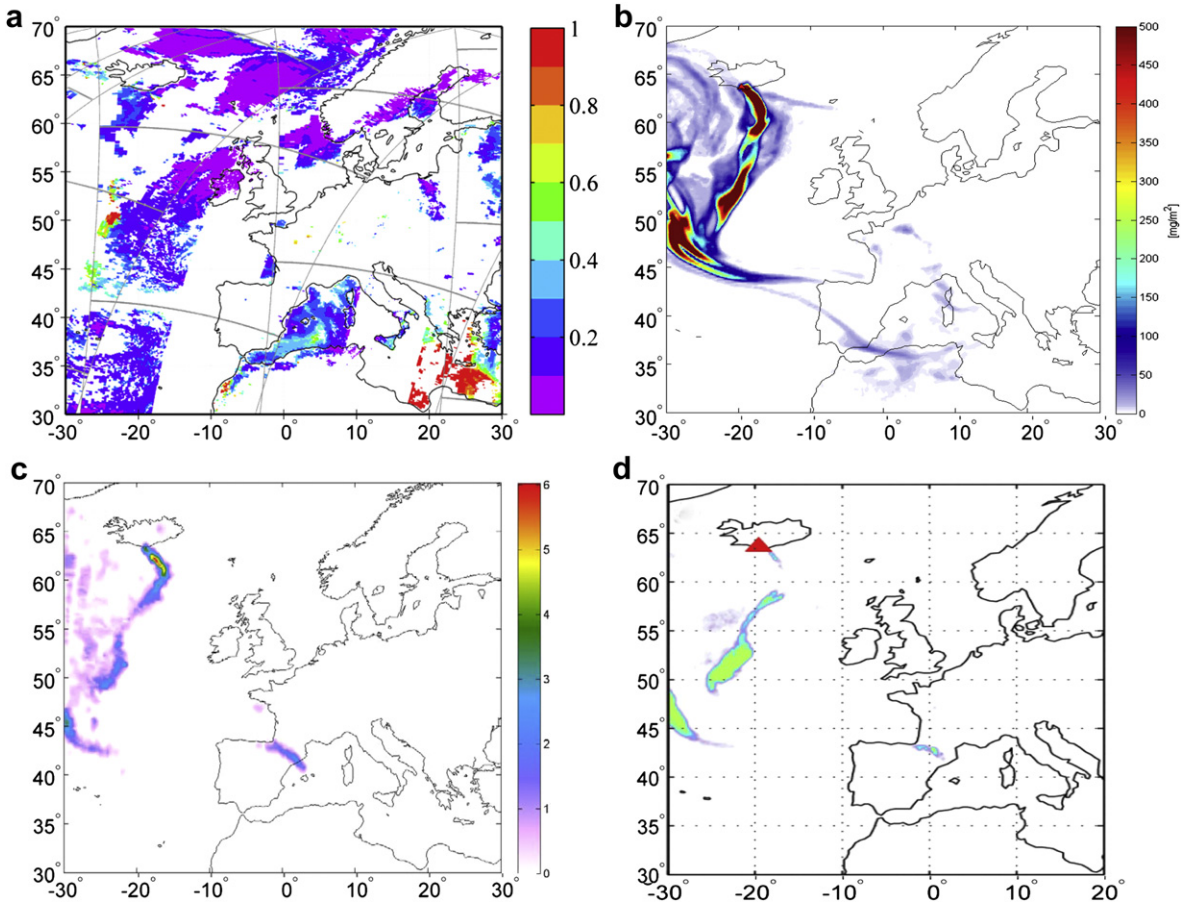

Fig. 4. (a) MODIS aerosol optical depth at 550 nm on 8 May 2010 (Terra); (b) FLEXPART simulation for column mass concentration at 0600UTC for particle size 0.75–2.5 μm; (c) Brightness temperature difference (K) from IASI satellite sensor at morning overpass (about 0930UTC); (d) Ash product from SEVIRI at 1000UTC.

by means of the geosynchronous Meteosat Second Generation (MSG) Spin-stabilised Enhanced Visible and Infrared Imager (SEVIRI) and the polar-orbiting MetOp Infrared Atmospheric Sounding Interferometer (IASI). The retrieval methodology is extensively described in Stohl et al. (2011) and references therein. Regarding SEVIRI, a large table of Top of the Atmosphere brightness temperature is calculated, from which the best fit effective particle radius and infrared optical depth can be estimated. Column mass (g m^{-2}) is estimated from the optical depth, assuming spherical shape and ash density. Such retrievals are svensitive to ash radii in the range 1–16 μm. As a measure for the total ash column, the Brightness Temperature Difference (BTD) between two IASI infrared channels (1231.5 cm^{-1} and 1160 cm^{-1}) was calculated. This BTD is close to zero for clear or cloudy observations and positive for ash scenes (Clarisse et al., 2010b).

The lidar observations at the EARLINET sites Evora and Granada (Guerrero-Rascado et al., 2010) were also used to confirm the presence of aerosol layers in the upper troposphere. These data, together with the rest of EARLINET sites, are reported by Pappalardo et al. (in preparation). The methodology applied for the aerosol layer identification and type assignment is described by Mona et al. (2011). Quicklooks of lidar data (range corrected signal) for a number of sites are available at http://www.meteo.physik.uni-muenchen.de/~stlidar/quicklooks/European-quicklooks.html.

The Lagrangian particle dispersion model FLEXPART was used to simulate the dispersion of volcanic aerosols (Stohl et al., 1998, 2005). The ash source term used by the model was constrained by satellite observations of volcanic ash, as described in Stohl et al. (2011). The simulations accounted for wet and dry deposition and gravitational settling, assuming an initial size distribution based on ash ground samples and in situ observations. FLEXPART was driven with 3-hourly meteorological data from two different sources (ECMWF and NCEP-GFS) to help quantifying model uncertainty but here only ECMWF-based model results are shown. For more details on the Eyjafjallajökull ash dispersion simulations see Stohl et al. (2011).

The column mass concentrations for 0.25–11 μm radius interval from FLEXPART were converted into (coarse mode) optical depth at 500 nm following the methodology described by Ansmann et al. (2011). For that, the mass extinction efficiency is estimated from an ash density of 2.6 g m^{-3} and volume extinction efficiency of 0.6 m^{-1} (500 nm wavelength), the latter value derived from actual AERONET observations (column volume concentrations and optical depths).

4. Results and discussion

The typical aerosol optical properties (AOD, AE, size distributions, SSA, seasonal patterns) over the Iberian Peninsula have been reported by several authors (see references in Table 1). An aerosol climatology based on sun photometer data for southwestern Spain was given by (Toledano et al., 2007a, 2009). The most noticeable feature is the occurrence of Saharan dust outbreaks that transport desert dust over the Iberian Peninsula on about 15–20% of all days (Toledano et al., 2007b). Depending on the synoptic conditions and season, different regions are affected (Escudero et al., 2005). Episodic biomass burning from forest fires affects the region, mainly in summer (Toledano et al., 2007a; Cachorro et al., 2008).

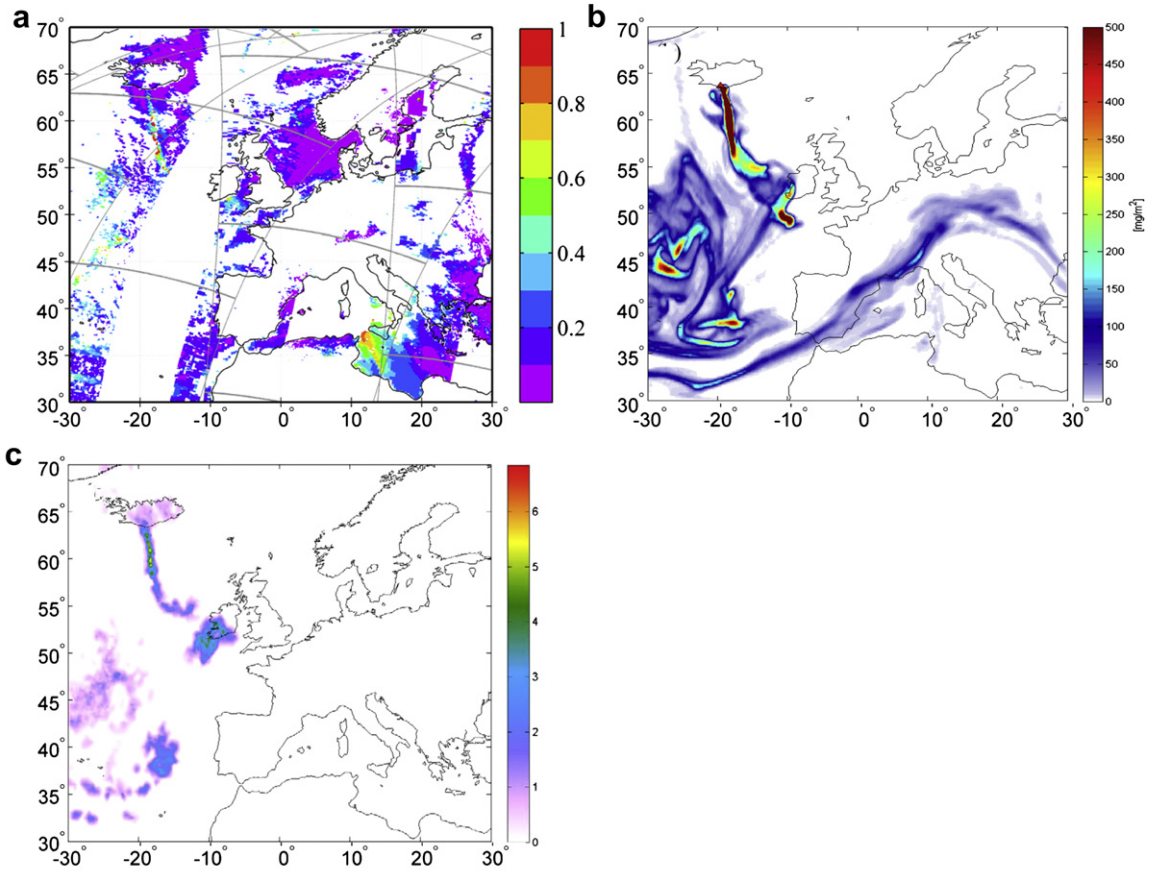

Fig. 5. a) MODIS aerosol optical depth at 550 nm on 11 May 2010 (Terra); (b) FLEXPART simulation for column mass concentration at 1200UTC for particle size 0.75–2.5 μm; (c) Brightness temperature difference (K) from IASI satellite sensor at morning overpass (about 0930UTC).

The set of measurements that indicated the transport of several ash clouds over the Iberian Peninsula during 6–12 May is presented in Section 4.1. In this context, the optical and microphysical aerosol properties derived from sun photometer were investigated (Sections 4.2 and 4.3) and compared to other AERONET sites in central Europe, that registered the first ash observations during 16–18 April. The satellite data and FLEXPART simulations were used to support interpretation.

4.1. Evidence of volcanic ash

The arrival of volcanic aerosols in the Iberian Peninsula on 6–12 May has been assessed by means of multiple instrumentation. Lidars within EARLINET reported in near real-time the arrival of elevated aerosol layers (Molero et al., 2010; Guerrero-Rascado et al., 2010; Pappalardo et al., 2010, in preparation) on 6–8 May 2010. The lidar systems in Granada (Fig. 3d) and Evora (not shown) revealed aerosol layers in the free troposphere at altitudes between 3 km and 6 km. The MODIS satellite sensor detected enhanced AOD levels over the Atlantic Ocean on 7 May (Fig. 3a), in agreement with the FLEXPART model simulation. Despite the gaps in the MODIS maps due to clouds (white areas in Fig. 3a), it is possible to see the main plume leaving the volcano, with optical depth (550 nm) about 1.0. High optical thickness was also detected west of France, about 50°N, 20°W, where the modeled ash total column loadings were very high. The ash arriving in the Iberian Peninsula from the southwest, visible in the FLEXPART simulation (Fig. 3b), had lower optical depth, about 0.4 as measured by MODIS over the Cadiz Gulf region, close to the Huelva site. Similar AOD values from MODIS were obtained on the Spanish Mediterranean coast. On this day, the IASI sensor showed the presence of ash over northwestern Spain, but not in the south. Note that these comparisons are highly qualitative since the different sensors provide different quantities: column AOD from MODIS is an optical measurement and cannot separate optical depth due to ash from other aerosols. From FLEXPART, we have extracted column mass for aerosols within the size range 0.75–2.5 μm. Furthermore, the MODIS plot includes measurements spanning several hours, whereas the FLEXPART simulation is a snapshot of the model output at the indicated time. A quantitative comparison is provided in Section 4.2.

On 8 May the first ash cloud reached the Mediterranean Spanish coast, as indicated by the high AOD (550 nm) from MODIS east of Spain and the FLEXPART simulation (Fig. 4). Another elongated ash puff crossed over northern Spain and is clearly shown by IASI and SEVIRI sensors (Fig. 4c and d). However this particular event was not captured by FLEXPART. This episode reveals the most outstanding discrepancy between the FLEXPART simulation and IASI and SEVIRI data for the entire Eyjafjallajökull eruption period.

According to FLEXPART, a second minor ash cloud reached southwestern Portugal on 10 May and crossed over the Iberian Peninsula on 11 May (Fig. 5), although the available satellite data cannot confirm this, probably because of insufficient sensitivity to such low ash column loadings (see discussion in Section 4.2). Right after that, a third puff passed southern Spain and the Gibraltar Strait (Fig. 6b) on 12 May. In this case, the ash (that also affected the Canary islands and Morocco) is visible in the MODIS AOD record and the IASI ash product (Fig. 6).

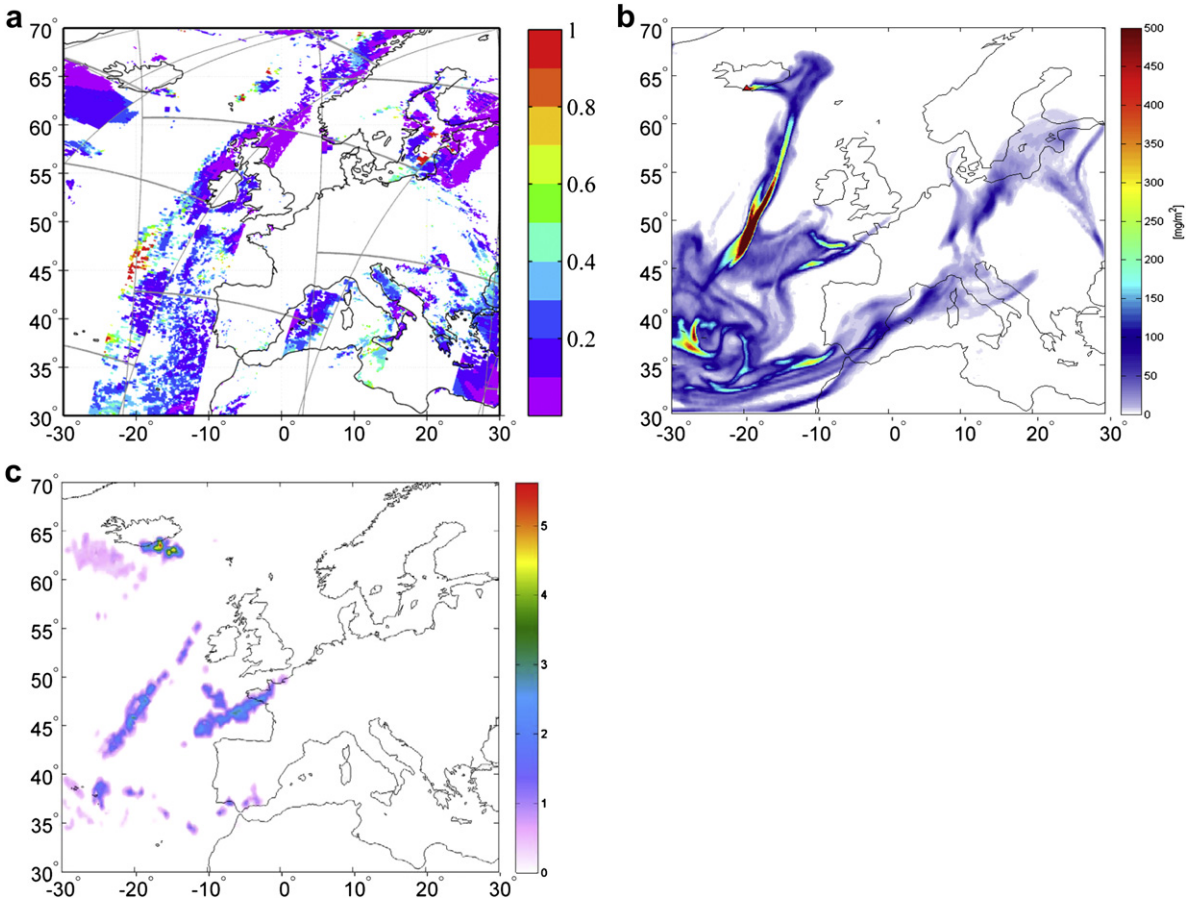

Fig. 6. a) MODIS aerosol optical depth at 550 nm on 12 May 2010 (Terra); (b) FLEXPART simulation for column mass concentration at 1800UTC for particle size 0.75–2.5 μm; (c) Brightness temperature difference (K) from IASI satellite sensor at morning overpass (about 0930UTC).

4.2. Ash optical thickness from sun photometer

Once the arrival of ash was evident, we investigated the data collected at the sun photometer sites. The AOD (440 nm) and AE time series are displayed in Fig. 7 for the 8 sites listed in Table 1. These parameters were used to identify aerosol types (Holben et al., 2001; Toledano et al., 2007a), with AOD accounting for the column load and the AE for the size predominance. The time series of AOD (550 nm) from MODIS, the column mass concentrations (g m^{-2}) from FLEXPART and the BTD (K) from IASI are superimposed in Fig. 7. Note that, despite the large gaps in the MODIS maps due to clouds, there are enough pixels with valid retrieval to provide the

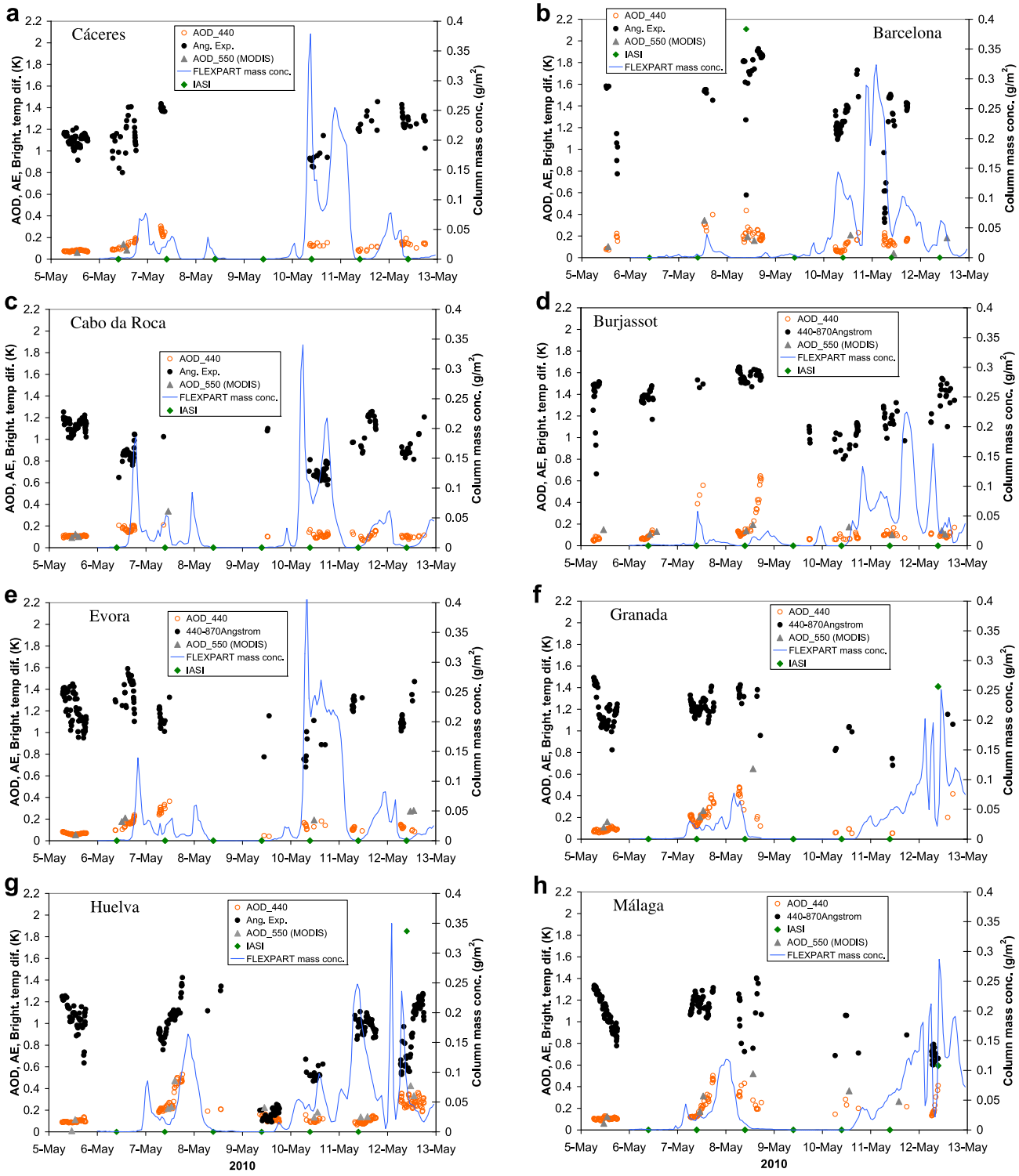

Fig. 7. Time series of Aerosol optical depth (440 nm) and Ångström exponent (440–870 nm) from AERONET, AOD (550 nm) from MODIS (Terra and Aqua), column mass concentrations (g m^{-2}) from FLEXPART simulations and IASI ash product (brightness temperature difference, in K) on 5–12 May 2010 at the AERONET-RIMA sites: (a) Cáceres; (b) Barcelona; (c) Cabo da Roca; (d) Burjassot; (e) Evora; (f) Granada; (g) Huelva; (h) Málaga.

AOD time series in most of the cases. Brightness temperature differences from IASI over the sites are zero except for Barcelona on 8 May and the southern sites on 12 May.

At all sites, the AOD on 5 May was low and stable. That day was used as a reference for the background aerosol at each site, since it indicated the aerosol present just before the arrival of volcanic aerosols in the free troposphere. An increase in the AOD was observed at the western sites (Cabo da Roca, Evora and Cáceres) already on 6 May, earlier in Cabo da Roca. The AOD increased up to 0.2 and the AE ranged from 0.7 at the coastal site Cabo da Roca up to 1.5 in the continental locations.

On 7 May the AOD increase was registered at the southern sites: Huelva, Granada and Málaga. The AOD (440 nm) rose strongly at these sites: 0.4 at Granada and 0.5 at Huelva and Málaga. The temporal agreement between the AOD and the FLEXPART concentration is good for these sites (Fig. 7f, g, h). The AE was stable around 1.2 (peaking at values of about 1.4), indicating the fine particle predominance in the atmospheric column. Due to clouds, few sun photometer data were available on 7 May at the Mediterranean sites (Burjassot and Barcelona), but the moderate AOD and high associated AE seem to indicate the presence of fine particles. On 8 May the AOD increased up to 0.62 at Burjassot but, due to the high AE (above 1.5), the coexistence of volcanic ash with local (urban) aerosols in the boundary layer cannot be discarded. At Barcelona, one single AOD observation at 10UTC about 0.4 coincides with the ash shown by IASI (BTD = 2.1 K) and SEVIRI (Fig. 4). At the southern sites, the AOD decreased during 8 May as the ash left.

Therefore the first puff as modeled by FLEXPART was detected with the sun photometers as it crossed from West to East. The increase of the AOD with respect to the background values was about 0.2–0.4 depending on the sites. The AE in the range 1–1.5 indicated the fine particle predominance within this puff. This feature was further investigated with the size distributions derived from inversions (Section 4.3).

According to the FLEXPART simulation (Fig. 5b), a second puff of ash arrived on 10 May and crossed over the Iberian Peninsula, arriving in the Mediterranean coast on 11 May. However the sun photometer sites did not exhibit any relevant increase on those days, except maybe at Barcelona (Fig. 7b), where the AE was as low as 0.33 in the morning. The ash experienced a longer transport path than the one arriving on previous days, and precipitation occurred that could have washed out the particles. The MODIS aerosol optical depth in Fig. 5 does not show the modeled ash either (maybe because of clouds), although there is agreement between MODIS observations and the model over the Atlantic ocean and the west of the UK.

On 12 May, a third puff of ash arrived in the southwestern part of the Iberian Peninsula. In this case the path from Iceland was shorter and the MODIS data over the Cadiz Gulf and south of the Balearic islands indicated enhanced AOD, about 0.3 at 550 nm wavelength (Fig. 6). The ash was observed at Huelva site (Fig. 7g) and maybe Málaga (Fig. 7h), in agreement with the model output. Note the lower AE observations on this day (about 0.55), that are indicative of larger portion of coarse particles.

In order to evaluate the agreement between model mass concentrations and sun photometer optical depths, the FLEXPART time series of mass concentration (integrated over the size range 0.25–11 μm) were converted into ash optical depth, as indicated in Section 3. These values were compared to the coarse mode optical depth as provided by the spectral deconvolution algorithm (O'Neill et al., 2003) applied to the AOD data. The coarse mode AOD (τ_c) peaks from both model and sun photometer (500 nm) during 6–8 and 11–12 May observations are given in Table 2. Despite the rough estimation, the τ_c has the same order of magnitude and the agreement is in some cases very good. During the 6–8 May event, the model tends to underestimate the τ_c (except for the mentioned peak in Barcelona). Conversely, during the 11–12 May event, model estimates are generally larger than the sun photometer observations. This simple approach demonstrated that the modeled mass concentrations can account for the observed coarse mode AOD increase. Besides, the fine/coarse mode AOD separation is another indicator of the arrival of fine particles (likely sulphates), that are not included in the FLEXPART simulation but that can have a major contribution in the observed AOD increase.

To summarize, the AOD analysis allowed identifying which ash puffs, as predicted by the model, actually crossed over the region. Second, the fine particles predominated in the 7–8 May event, although the wide range and variability of AE revealed dramatic and sometimes quick changes in mean particle size (e.g. Huelva on 12 May, Fig. 7g). All observations were made in ash clouds with relatively low ash column loadings compared to those present over the North Atlantic at the same time. However, ash clouds with higher ash column loadings were never transported across the Iberian Peninsula.

4.3. Inversion-derived properties

The AERONET inversion of sun–sky radiance data provided information on the particle size distribution, single scattering albedo and complex refractive index. In a similar way to the AOD analysis, the results from these parameters on 5 May were used as a reference value for the local aerosol at each site. The optical and microphysical parameters for the investigated days are given in Table 3.

The particle size distributions are shown in Fig. 8 for different dates of interest (see Table 3) at four sites. The reference value before the arrival of the ash (the average on 5 May) is also depicted. In general the arrival of volcanic ash produced enhanced concentrations in both the fine and the coarse modes, the fine mode fraction (FMF) ranging from 0.19 to 0.79 with average of 0.41. The increase in volume concentrations is about one order of magnitude (e.g. 8 May at Granada and Huelva) and quite even in both modes. Similar behavior was encountered, for example, at Chilbolton site (England) on 19 April during the first Eyjafjallajökull eruptive phase (see data on the AERONET website).

However in few cases, the size distributions indicated something different. At Evora (7 May, Fig. 8a) and Huelva (12 May, Fig. 8c) the coarse mode predominance is evident, with the lowest FMF's (0.19 and 0.26). The coarse particle predominance was also observed during April event at various AERONET sites in Europe (e.g. Dunkerke 18 April), with low associated Ångström exponents <0.7. Conversely the FMF at Burjassot was very high (0.79) and the size distribution basically changed in the fine mode only, not showing an increase of the coarse mode concentration (Fig. 8b).

Table 2
Coarse mode aerosol optical depth (τ_c) peaks during the observation periods 6–8 and 11–12 May over the AERONET sites derived from AERONET data (O'Neill et al., 2003) and from FLEXPART mass concentrations, applying the conversion factors given by Ansmann et al. (2011)

Site	6–8 May		11–12 May	
	$\tau_{c(AERONET)}$	$\tau_{c(FLEXPART)}$	$\tau_{c(AERONET)}$	$\tau_{c(FLEXPART)}$
Barcelona	0.24	0.02	0.16	0.20
Burjassot	0.07	0.04	0.04	0.14
Cabo da Roca	0.10	0.12	0.08	0.21
Cáceres	0.07	0.05	0.06	0.05
Evora	0.12	0.09	0.05	0.05
Granada	0.10	0.05	0.15	0.16
Huelva	0.17	0.10	0.20	0.22
Málaga	0.15	0.07	0.20	0.18

Table 3
Summary of AOD at 440 nm (τ_{440}), Ångström exponent of extinction (AE or α_{ext}) and aerosol properties retrieved with the Dubovik inversion: volume concentrations for the fine and coarse modes (V_f and V_c, in $\mu m^3\ \mu m^{-2}$), fine mode fraction (FMF), single scattering albedo at 440 and 1020 nm (ω_{0-440} and ω_{0-1020}), Ångström exponent of absorption (α_{abs}), portion of spherical particles (C_{sph} in %), real and imaginay parts of the refractive index at 440 nm (n_{440},k_{440}) and number of inversions (N).

Site	date	τ_{440}	α_{ext}	V_f	V_c	FMF	ω_{0-440}	ω_{0-1020}	α_{abs}	C_{sph}	n_{440}	k_{440}	N
Barcelona	7 May	0.31	1.52	N/A	N/A	N/A	N/A	N/A	N/A	N/A	N/A	N/A	0
Burjassot	8 May	0.23	1.58	0.066	0.018	0.79	0.95	0.9	0.89	99	1.45	0.008	4
Cabo da Roca	6–7 May	0.17	0.87	0.019	0.053	0.26	0.97	0.97	0.89	13	1.47	0.002	3
Cáceres	6–7 May	0.17	1.21	0.028	0.032	0.47	N/A	N/A	0.82	33	N/A	N/A	3
Evora	6–7 May	0.22	1.3	0.022	0.039	0.36	0.95	0.95	1.12	31	1.48	0.005	5
Granada	7–8 May	0.25	1.25	0.055	0.059	0.48	0.98	0.97	0.86	37	1.41	0.002	5
Huelva	08-may	0.31	1.04	0.078	0.093	0.46	0.97	0.97	1.10	55	1.38	0.002	3
	12 may	0.28	0.91	0.024	0.104	0.19	0.92	0.89	0.35	60	1.49	0.005	2
Málaga	7–8 May	0.23	1.16	0.035	0.076	0.32	0.96	0.94	0.85	82	1.54	0.004	2
	12 may	0.19	0.7	0.013	0.026	0.33	N/A	N/A	N/A	87	N/A	N/A	3

Because of this, we suspect that local aerosols (urban pollution) constituted the main aerosol type at this particular site and it masked the volcanic aerosol properties.

Volcanic stratospheric aerosols exhibited a distinct feature, that was detected in the early AERONET observations in 1993–1994, after the eruption of Mount Pinatubo: the retrieved size distributions had an extra mode centered at about 0.5 μm radius (Eck et al., 2010). This mode appeared in between the two classical modes of tropospheric aerosols, resulting in trimodal size distributions. During our case study in May 2010 of the Eyjafjallajökull eruption, such features were not observed. According to the plume height observations by radar close to the volcano and by lidar stations in Europe, the aerosols were injected and transported mostly within the troposphere. The size distributions from sun photometer are also typical of tropospheric aerosols.

Note that in this section the fine mode fraction is evaluated from the size distributions. However, similar volume concentrations of the fine and coarse mode yield to fine particle predominance in the optical properties (high AE above 1, see Table 3), since these parameters are sensitive to the particle number.

The single scattering albedo as a function of wavelength is depicted in Fig. 9. This representation is very useful to identify aerosol types, following the climatology reported by Dubovik et al. (Dubovik et al., 2002). During the 6–8 May event, the absorption was rather low and nearly wavelength independent within the investigated range (440–1020 nm). Interestingly, such values could only be comparable to some type of anthropogenic pollution (sulphates) or marine aerosols (representative sites are GSFC and Lanai respectively, see Fig. 1 of (Dubovik et al., 2002)). But the AE of urban/industrial aerosols should be higher (>1.7), and the observed aerosol cannot consist of maritime particles with such high AOD. Therefore a distinct aerosol type could be encountered here, although the SSA uncertainty (±0.03) in the AERONET retrieval does not allow to reach definitive conclusions.

The lowest SSA values were found at Huelva (12 May), associated to coarse particle predominance. However the SSA wavelength dependence is different from the typical dust observations. This fact allows discarding the presence of Saharan dust over the site and is in agreement with the general atmospheric flow (from the northwest). Finally, the larger SSA slope at Burjassot differs from the

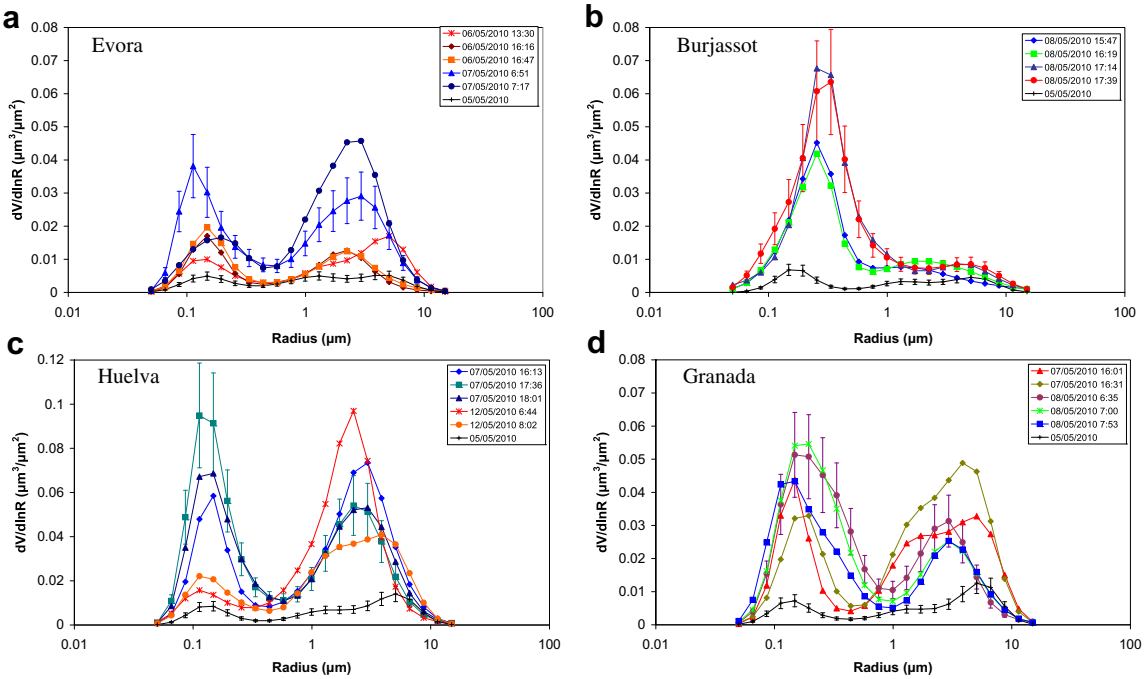

Fig. 8. Volume particle size distributions derived from the inversion of sun-sky radiometer data at four representative sites: (a) Evora; (b) Burjassot; (c) Huelva; (d) Granada. Error bars are added to the reference case and one of the ash cases for illustration.

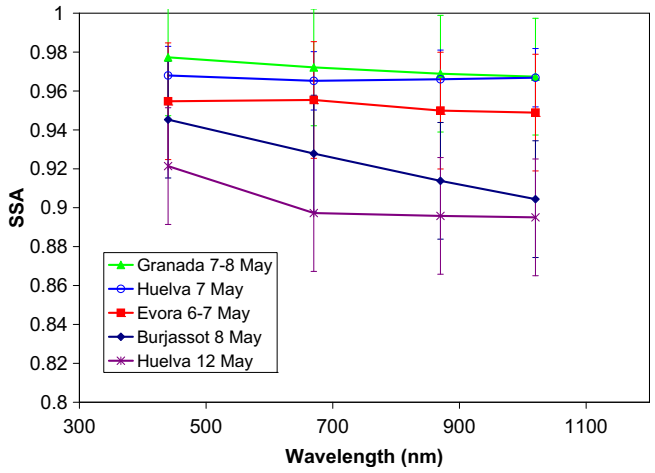

Fig. 9. Single scattering albedo (daily averages) as a function of wavelength for various sun photometer sites during the volcanic aerosol event on 6–12 May 2010. Bars indicate measurement uncertainty.

other sites. Given the similarity with the expected spectral SSA values for mixtures that include combustion aerosols, this is another confirmation that at Burjassot the volcanic ash was not the predominant aerosol type.

The absorption Ångström exponent (AAE), calculated in the range 440–870 nm from the absorption aerosol optical depth, is also included in Table 3. This parameter typically exhibits high values (about 2.0 or larger) for desert dust, and about 1 if black carbon is the main absorber. The AAE observed in this episode was very low, with a mean α_{abs} of 0.93 on 6–8 May. Such low values are rare in the literature (Russell et al., 2010). Note, however, that the uncertainty associated to this parameter is very high. If the typical retrieval errors are assumed (uncertainties about 0.03 for SSA, 0.02 for AOD), the AAE error exceeds 30–50% even for moderate AOD values. Furthermore, the AAE on 12 May was really low (0.40). Such low values can be explained by the wavelength independency of optical properties in case of very large particles ($r > 10$–15 μm).

The portion of spherical particles (C_{sph}) was very variable, with mean value of 55%. Finally the refractive index was in average $1.47 + 0.005125i$. The real part was lower than it is reported for dust, about 1.55 (e.g. Petzold et al. (2009)) and higher than that of urban aerosols, about 1.40 (Dubovik et al., 2002). In general this parameter experienced a decrease with respect to the values on 5 May when the volcanic ash arrived. As for the AAE and refractive index, the error associated to these optical parameters is large and the measurements must be interpreted with caution.

Finally note that the contribution of boundary layer aerosols (or even other long-range transported aerosols) to the total column was not negligible and its possible variations could be responsible for some of the observed changes in the columnar optical properties. The ash column loadings were never high enough to allow neglecting the other aerosols.

5. Conclusions

The volcanic ash concentration simulated with the FLEXPART model was investigated by means of ground-based sunphotometry and satellite remote sensing. Specific ash products from IASI and SEVIRI, as well as AOD and coarse mode concentrations of the size distributions from AERONET-RIMA sun photometers, were used to identify the volcanic aerosols. The simulated ash on 6–8 May and 12 May was detected, but not the one on 10–11 May. The longer and more complicated path over the Atlantic of this ash cloud, and likely removal processes (precipitation), may not have been well captured by FLEXPART.

Within the detected volcanic aerosols, the sun-sky radiance data collected by the AERONET-RIMA sun photometers provided information on the optical and microphysical properties. The volcanic aerosols on 6–8 May over the Iberian Peninsula had a relevant fine mode volume fraction (0.41) and portion of non-spherical particles (40–60%). The single scattering albedo was high (0.95 at 440 nm) and showed a slight decrease with wavelength. If these properties are put together with the moderate AOD (0.3–0.5 at 440 nm), the intermediate Ångström exponent of extinction (1–1.4) and low absorption Ångström exponent (about 0.9), the aerosol type seems to have distinct properties, different from those of other natural or anthropogenic aerosols.

However the ash on 12 May, only detected at the southernmost sites, had larger portion of coarse particles and somewhat different properties (more absorbing, lower AAE) than the observations on 6–8 May. When compared with the AERONET measurements collected in the vicinity of the English Channel during the April eruption, both types of scenarios (fine particle and coarse particle dominated) were found among the data. The variability encountered among sites during the different days indicated that the puffs of ash were rather inhomogeneous with respect to particle mean size and shape. It must be noted, though, that variations in the boundary layer aerosols might be responsible for some of these changes. Nevertheless, a significant increase of the coarse mode concentration was detected in all cases, indicating the arrival of coarse ash particles.

The coincidence with Saharan dust was discarded by the analysis of the AOD, single scattering albedo wavelength dependency and air mass origin. The presence of volcanic stratospheric aerosols (e.g. third mode in the size distribution with particles about 0.5 μm) was not detected.

The sites equipped with multiple instrumentation have notable capabilities in this kind of events. However many AERONET sites exist where no other instruments operate, and our analysis can provide guidance for interpretation of volcanic aerosol data in such cases. The site location in remote areas, where local aerosol sources are negligible, is highly desirable. The number of stations over the Iberian Peninsula allowed to identify temporal patterns, that were also helpful to distinguish transported from local aerosols.

Acknowledgments

This work was funded by CICYT under projects CGL2009-09740, CGL2010-09480-E and CGL2008-05939. We thank the AERONET, PHOTONS and RIMA staff for their scientific and technical support. We are also grateful to the members of the NASA MODIS science team for providing the data used in this study. We thank the staff of the CIECEM (http://www.ciecem.uhu.es) for their help in maintaining Huelva site.

References

Ansmann, A., Tesche, M., Groß, S., Freudenthaler, V., Seifert, P., Hiebsch, A., Schmidt, J., Wandinger, U., Mattis, I., Müller, D., Wiegner, M., 2010. The 16 April 2010 major volcanic ash plume over central Europe: EARLINET lidar and AERONET photometer observations at Leipzig and Munich, Germany. Geophysical Research Letters 37, L13810.

Ansmann, A., Tesche, M., Seifert, P., Gross, S., Freudenthaler, V., Apituley, A., Wilson, K.M., Serikov, I., Linne, H., Heinold, B., Hiebsch, A., Schnell, F., Schmidt, J., Mattis, I., Wandinger, U., Wiegner, M., Ash and fine-mode particle mass profiles from EARLINET-AERONET observations over central Europe after the eruptions of the Eyjafjallajökull volcano in 2010, Journal of Geophysical Research 116, D00U02, doi:10.1029/2010JD015567.

Basart, S., Pérez, C., Cuevas, E., Baldasano, J.M., Gobbi, G.P., 2009. Aerosol characterization in Northern Africa, Northeastern Atlantic, Mediterranean Basin and Middle east from direct-sun AERONET observations. Atmospheric Chemistry and Physics 9, 8265–8282.

Bennett, A.J., Odams, P., Edwards, D., Arason, P., 2010. Monitoring of lightning from the April–May 2010 Eyjafjallajökull volcanic eruption using a very low frequency lightning location network. Environment Reserch Letters 5, 044013.

Bennouna, Y., Cachorro, V., Toledano, C., Berjón, A., Prats, N., Fuertes, D., Gonzalez, R., Rodrigo, R., Torres, B., de Frutos, A., 2011. Comparison of atmospheric aerosol climatologies over southwestern Spain derived from AERONET and MODIS. Remote Sensing of Environment 115, 1272–1284.

Cachorro, V.E., Toledano, C., Prats, N., Sorribas, M., Mogo, S., Berjon, A., Torres, B., Rodrigo, R., de la Rosa, J., de Frutos, A.M., 2008. The strongest desert dust intrusion mixed with smoke over the Iberian Peninsula registered with Sun photometry. Journal of Geophysical Research 113, D14504.

Clarisse, L., Hurtmans, D., Prata, A.J., Karagulian, F., Clerbaux, C., De Maziere, M., Coheur, P.F., 2010a. Retrieving radius, concentration, optical depth, and mass of different types of aerosols from high-resolution infrared nadir spectra. Applied Optics 49, 3713–3722.

Clarisse, L., Prata, F., Lacour, J.L., Hurtmans, D., Clerbaux, C., Coheur, P.F., 2010b. A correlation method for volcanic ash detection using hyperspectral infrared measurements. Geophysical Research Letters 37, L19806.

Dubovik, O., King, M., 2000. A flexible inversion algorithm for retrieval of aerosol optical properties from sun and sky radiance measurements. Journal of Geophysical Research 105, 20,673–20,696.

Dubovik, O., Smirnov, A., Holben, B.N., King, M.D., Kaufman, Y.J., Eck, T.F., Slutsker, I., 2000. Accuracy assessments of aerosol optical properties retrieved from Aerosol Robotic Network (AERONET) Sun and sky radiance measurements. Journal of Geophysical Research 105, 9791–9806.

Dubovik, O., Holben, B., Eck, T., Smirnov, A., Kaufman, Y., King, M.D., Tanre, D., Slutsker, I., 2002. Variability of absorption and optical properties of key aerosol types observed in worldwide locations. Journal of the Atmospheric Sciences 59, 590–608.

Dubovik, O., Sinyuk, A., Lapyonok, T., Holben, B.N., Mishchenko, M., Yang, P., Eck, T.F., Volten, H., Mu noz, O., Veihelmann, B., van der Zande, W.J., Léon, J.F., Sorokin, M., Slutsker, I., 2006. Application of spheroid models to account for aerosol particle nonsphericity in remote sensing of desert dust. Journal of Geophysical Research 111, D11208.

Eck, T.F., Holben, B.N., Siniuk, A., Pinker, R.T., Goloub, P., Chen, H., Chatenet, B., Li, Z., Singh, R.P., Tripathi, S.N., Reid, J.S., Giles, D.M., Dubovik, O., O'Neill, N.T., Smirnov, A., 2010. Climatological aspects of the optical properties of fine/coarse mode aerosol mixtures. Journal of Geophysical Research 115, D19205.

Elias, T., Silva, A.M., Belo, N., Pereira, S., Formenti, P., Helas, G., Wagner, F., 2006. Aerosol extinction in a remote continental region of the Iberian Peninsula during summer. Journal of Geophysical Research 111, D14204.

Escudero, M., Castillo, S., Querol, X., Avila, A., Alarcon, M., Viana, M.M., Alastuey, A., Cuevasn, E., Rodriguez, S., 2005. Wet and dry African dust episodes over eastern Spain. Journal of Geophysical Research 110, D18S08.

Estellés, V., Martínez-Lozano, J.A., Utrillas, M.P., Campanelli, M., 2007. Columnar aerosol properties in Valencia (Spain) by ground-based Sun photometry. Journal of Geophysical Research 112, D11201.

Flentje, H., Claude, H., Elste, T., Gilge, S., Köhler, U., Plass-Dülmer, C., Steinbrecht, W., Thomas, W., Werner, A., Fricke, W., 2010. The Eyjafjallajökull eruption in April 2010 – detection of volcanic plume using in-situ measurements, ozone sondes and lidar-ceilometer profiles. Atmospheric Chemistry and Physics 10, 10085–10092.

Foyo-Moreno, I., Alados, I., Lyamani, H., Olmo, F.J., Alados-Arboledas, L., 2010. Aerosols characterization in the western Mediterranean (Málaga, Spain). In: Sobrino, J.A. (Ed.), Third Recent Advances in Quantitative Remote Sensing pp. 16–20.

Guerrero-Rascado, J.L., Sicard, M., Molero, F., Navas-Guzmán, F., Preißler, J., Kumar, D., Bravo-Aranda, J.A., Tomás, S., Reba, M.N., Alados-Arboledas, L., Comerón, A., Pujadas, M., Rocadenbosch, F., Silva, F.W.A.M., 2010. Monitoring of the Eyjafjalla Volcanic Plume at Four Lidar Stations over the Iberian Peninsula: 6 to 8 May 2010 IV Reunión Española de Ciencia y Tecnologìa del aerosol – RECTA.

Holben, B., Eck, T., Slutsker, I., Tanré, D., Buis, J., Setzer, A., Vermote, E., Reagan, J., Kaufman, Y., 1998. AERONET – a federated instrument network and data archive for aerosol characterization. Remote Sensing of Environment 66, 1–16.

Holben, B., Tanre, D., Smirnov, A., Eck, T., Slutsker, I., Abuhassan, N., Newcomb, W., Schafer, J., Chatenet, B., Lavenue, F., Kaufman, Y., Vande Castle, J., Setzer, A., Markham, B., Clark, D., Frouin, R., Halthore, R., Karnieli, A., O'Neill, N., Pietras, C., Pinker, R., Voss, K., Zibordi, G., 2001. An emerging ground-based aerosol climatology: aerosol Optical Depth from AERONET. Journal of Geophysical Research 106, 12067–12097.

Levy, R., Remer, L., Tanrè, D., Mattoo, S., Kaufman, Y., 2009. Algorithm for Remote Sensing of Tropospheric Aerosol over Dark Targets from MODIS: Collection 005 and 051: Revision 2. http://modis-atmos.gsfc.nasa.gov/_docs/ATBD_MOD04_C005_rev2.pdf.

Lyamani, H., Olmo, F., Alados-Arboledas, L., 2004. Long-term changes in aerosol radiative properties at Armilla (Spain). Atmospheric Environment 38, 5935–5943.

Lyamani, H., Olmo, F., Alados-Arboledas, L., 2005. Saharan dust outbreak over southeastern Spain as detected by sun photometer. Atmospheric Environment 39, 7276–7284.

Minnis, P., Harrison, E.F., Stowe, L.L., Gibson, G.G., Denn, F.M., Doelling, D.R., Smith, W.L., 1993. Radiative climate Forcing by the Mount Pinatubo eruption. Science 259, 1411–1415.

Molero, F., Sicard, M., Guerrero-Rascado, J., Navas-Guzmán, F., Tomás, S., Preißler, J., Kumar, D., Rocadenbosch, F., Alados-Arboledas, L., Wagner, F., Comeron, A., Pujadas, M., 2010. Comparison of SPALINET Network Lidar Measurements with Models Forecast during the Eyjafjalla Event ILRC'10, Saint-Petersburg, Russia.

Mona, L., Amodeo, A., D'Amico, G., Giunta, A., Madonna, F., Pappalardo, G., 2011. Multi-wavelength Raman lidar observations of the Eyjafjallajökull volcanic cloud over Potenza, Southern Italy. Atmospheric Chemistry and Physics Discussions 11, 12763–12803.

Obregón, M., Serrano, A., Cancillo, M., 2009. Application of different classifications to aerosols in column at Caceres. In: Proc. APMG 2009, 6ž Simpósio de Meteorologia e Geofisica da APMG / 10ž Encontro Luso-Espanhol de Meteorologia.

O'Neill, N.T., Eck, T.F., Smirnov, A., Holben, B.N., Thulasiraman, S., 2003. Spectral discrimination of coarse and fine mode optical depth. Journal of Geophysical Research 108 (D17), 4559.

Pappalardo, G., Mattis, I., collaborators, 2010. Dispersion and evolution of the Eyjafjallajökull ash plume over Europe: vertically resolved measurements with the European LIDAR network EARLINET. EGU General Assembly 2010. Geophysical Research Abstracts 12 EGU2010–15731.

Pappalardo, G., Mona, L., Adam, M., Apituley, A., Arboledas, L.A., Chaikovsky, A., Cuesta, J., de Tomasi, F., D'Amico, G., Giannakaki, E., Grigorov, I., Gross, S., Iarlori, M., Mamouri, R.E., Mattis, I., Mitev, V., Nicolae, D., Pietruczuk, A., Serikov, I., Sicard, M., Simenov, V., Spinelli, N., Trickl, T., Wagner, F., 4D distribution of the 2010 Eyjafjallajökull volcanic cloud over Europe observed by EARLINET. Atmospheric Chemistry and Physics, in preparation.

Petersen, G.N., 2010. A short meteorological overview of the Eyjafjallajökull eruption 14 April–23 May 2010. Weather 65, 203–207.

Petzold, A., Rasp, K., Weinzierl, B., Esselborn, M., Hamburger, T., Dörnbrack, A., Kandler, K., Schütz, L., Knippertz, P., Fiebig, M., Virkkula, A., 2009. Saharan dust absorption and refractive index from aircraft-based observations during SAMUM 2006. Tellus 61B, 118–130.

Prata, A.J., Grant, I.F., 2001. Retrieval of microphysical and morphological properties of volcanic ash plumes from satellite data: application to Mt. Ruapehu, New Zealand. Quarterly Journal of the Royal Meteorological Society 127, 2153–2179.

Russell, P.B., Bergstrom, R.W., Shinozuka, Y., Clarke, A.D., DeCarlo, P.F., Jimenez, J.L., Livingston, J.M., Redemann, J., Dubovik, O., Strawa, A., 2010. Absorption Angstrom Exponent in AERONET and related data as an indicator of aerosol composition. Atmospheric Chemistry and Physics 10 (3), 1155–1169.

Schumann, U., Weinzierl, B., Reitebuch, O., Schlager, H., Minikin, A., Forster, C., Baumann, R., Sailer, T., Graf, K., Mannstein, H., Voigt, C., Rahm, S., Simmet, R., Scheibe, M., Lichtenstern, M., Stock, P., Rüba, H., Schäuble, D., Tafferner, A., Rautenhaus, M., Gerz, T., Ziereis, H., Krautstrunk, M., Mallaun, C., Gayet, J.F., Lieke, K., Kandler, K., Ebert, M., Weinbruch, S., Stohl, A., Gasteiger, J., Groß, S., Freudenthaler, V., Wiegner, M., Ansmann, A., Tesche, M., Olafsson, H., Sturm, K., 2011. Airborne observations of the Eyjafjalla volcano ash cloud over Europe during air space closure in April and May 2010. Atmospheric Chemistry and Physics 11, 2245–2279.

Stohl, A., Hittenberger, M., Wotawa, G., 1998. Validation of the Lagrangian particle dispersion model FLEXPART against large scale tracer experiment data. Atmospheric Environment 32, 4245–4264.

Stohl, A., Forster, C., Frank, A., Seibert, P., Wotawa, G., 2005. Technical note: the Lagrangian particle dispersion model FLEXPART version 6.2. Atmospheric Chemistry and Physics 5, 2461–2474.

Stohl, A., Prata, A.J., Eckhardt, S., Clarisse, L., Durant, A., Henne, S., Kristiansen, N.I., Minikin, A., Schumann, U., Seibert, P., Stebel, K., Thomas, H.E., Thorsteinsson, T., Tørseth, K., Weinzierl, B., 2011. Determination of time- and height-resolved volcanic ash emissions for quantitative ash dispersion modeling: the 2010 Eyjafjallajökull eruption. Atmospheric Chemistry and Physics 11, 4333–4351.

Toledano, C., Cachorro, V.E., Berjon, A., de Frutos, A.M., Sorribas, M., de la Morena, B.A., Goloub, P., 2007a. Aerosol optical depth and Angstrom exponent climatology at El Arenosillo AERONET site (Huelva, Spain). Quarterly Journal of the Royal Meteorological Society 133, 795–807.

Toledano, C., Cachorro, V.E., de Frutos, A.M., Sorribas, M., Prats, N., de la Morena, B.A., 2007b. Inventory of African desert dust events over the southwestern Iberian Peninsula in 2000-2005 with an AERONET Cimel Sun photometer. Journal of Geophysical Research 112, D21201.

Toledano, C., Wiegner, M., Garhammer, M., Seefeldner, M., Gasteiger, J., Müller, D., Koepke, P., 2009. Spectral aerosol optical depth characterization of desert dust during SAMUM 2006. Tellus 61B, 216–228.

Wiegner, M., Gasteiger, J., Groß, S., Schnell, F., Freudenthaler, V., Forkel, R., Characterization of the Eyjafjallajökull ash-plume: Potential of lidar remote sensing. Physics and Chemistry of the Earth, in press.